



An evaluation of  
different dry  
deposition schemes

D. Wen et al.

# An evaluation of ambient ammonia concentrations over southern Ontario simulated with different dry deposition schemes within STILT-Chem v0.8

D. Wen<sup>1</sup>, L. Zhang<sup>2</sup>, J. C. Lin<sup>1,3</sup>, R. Vet<sup>2</sup>, and M. D. Moran<sup>2</sup>

<sup>1</sup>Waterloo Atmosphere–Land Interactions Research Group, Department of Earth and Environmental Sciences, University of Waterloo, Waterloo, Ontario, Canada

<sup>2</sup>Air Quality Research Division, Science and Technology Branch, Environment Canada, Toronto, Ontario, Canada

<sup>3</sup>Department of Atmospheric Sciences, University of Utah, Salt lake city, Utah, USA

Received: 6 October 2013 – Accepted: 8 November 2013 – Published: 29 November 2013

Correspondence to: J. C. Lin (john.lin@utah.edu)

Published by Copernicus Publications on behalf of the European Geosciences Union.

Title Page

Abstract

Introduction

Conclusions

References

Tables

Figures



Back

Close

Full Screen / Esc

Printer-friendly Version

Interactive Discussion



## Abstract

A bi-directional air-surface exchange scheme for atmospheric ammonia was incorporated into the Stochastic Time-Inverted Lagrangian Transport air quality model (STILT-Chem v0.8). STILT-Chem v0.8 was then applied to simulate atmospheric ammonia concentrations at 53 measurement sites in the province of Ontario, Canada for a six-month period from 1 June to 30 November 2006. In addition to the bi-directional scheme, two uni-directional dry deposition schemes were tested. Comparisons of modeled ammonia concentrations against observations show that all three schemes can reasonably predict observations. For sites with low observed ammonia concentrations, the bi-directional scheme clearly overestimated ammonia concentrations. Although all three schemes tend to underestimate ammonia concentrations for locations with elevated observed concentrations, the bi-directional scheme performed better due mainly to its introduction of compensation points into flux calculation parameterizations. The results of additional sensitivity tests suggest that uncertainties in the input values of emission potentials in the bi-directional scheme greatly affect the accuracy of modeled ammonia concentrations. The use of much larger emission potentials than provided in the scheme is required for accurate prediction of elevated ammonia concentrations at intensive agricultural locations.

## 1 Introduction

As the primary basic gas in the atmosphere, atmospheric ammonia ( $\text{NH}_3$ ) plays an important role in several biogeochemical processes (Seinfeld and Pandis, 2006). It acts as a major agent in neutralizing acids in the atmosphere and substantially contributes to fine particulate matter ( $\text{PM}_{2.5}$ ) concentrations, which has impacts on air quality, acid deposition, atmospheric visibility, and climate. For example, human morbidity has been shown to increase linearly with PM concentrations (Pope et al., 2009), and excessive

GMDD

6, 6075–6115, 2013

### An evaluation of different dry deposition schemes

D. Wen et al.

Title Page

Abstract

Introduction

Conclusions

References

Tables

Figures

⏪

⏩

◀

▶

Back

Close

Full Screen / Esc

Printer-friendly Version

Interactive Discussion



deposition of atmospheric NH<sub>3</sub> and ammonium may lead to soil acidification and damage to sensitive species and ecosystem health (Morris, 1991; Van Bremen et al., 1982).

Unlike most gas-phase atmospheric species, which are predominantly either deposited to or emitted from the surface, NH<sub>3</sub> is a semi-volatile species and exhibits bi-directional exchange between the atmosphere and the Earth's surface. However, dry deposition and emission of NH<sub>3</sub> are simulated entirely separately in most atmospheric NH<sub>3</sub> modeling studies (Simpson et al., 2012; Vieno et al., 2010; Geels et al., 2012). Such a decoupled treatment of these two processes is less realistic than a combined, bi-directional, gradient-driven flux model. Simulations with separate representations of emission and dry deposition likely underestimate ambient NH<sub>3</sub> concentrations (Wichink Kruit et al., 2012). Thus, the development and application of bi-directional modeling of NH<sub>3</sub> is important since it is responsive to combined changes of these two processes and allows for more accurate estimation of surface fluxes. Significant efforts have been made in the past two decades to develop bi-directional NH<sub>3</sub> flux models (Sutton et al., 1998; Nemitz et al., 2001; Wu et al., 2009; Cooter et al., 2010; Kruit et al., 2010; Zhang et al., 2010).

Most existing bi-directional flux models for NH<sub>3</sub> were parameterized for applications at canopy scales (Flechard et al., 2013). Only a few models were developed for implementation in regional-scale air quality models due to the lack of required input parameters over a large number of different land-use categories (Kruit et al., 2010; Wichink Kruit et al., 2012; Cooter et al., 2010, 2012; Bash et al., 2013; Pleim et al., 2013). For example, required inputs of ground and stomatal emission potentials are generally not measured at regional scales or not explicitly calculated in regional scale models. Zhang et al. (2010) developed a bi-directional exchange model for NH<sub>3</sub> that can be easily implemented in any regional-scale air quality model: the required inputs of stomatal and ground emission potentials were empirically derived for different land-use categories based on an extensive literature review.

Although bi-directional exchange models of NH<sub>3</sub> are more mechanistically realistic in principle, few studies have examined their actual performances against uni-directional

## An evaluation of different dry deposition schemes

D. Wen et al.

Title Page

Abstract

Introduction

Conclusions

References

Tables

Figures



Back

Close

Full Screen / Esc

Printer-friendly Version

Interactive Discussion



## An evaluation of different dry deposition schemes

D. Wen et al.

Title Page

Abstract

Introduction

Conclusions

References

Tables

Figures

⏪

⏩

◀

▶

Back

Close

Full Screen / Esc

Printer-friendly Version

Interactive Discussion



dry deposition models at multiple measurement sites with a variety of different levels of  $\text{NH}_3$ . In this study, the bi-directional exchange scheme of Zhang et al. (2010) was implemented in the Stochastic Time-Inverted Lagrangian Transport air quality model (STILT-Chem v0.8). The model was then used to simulate  $\text{NH}_3$  concentrations at 53 measurement sites in southern Ontario, Canada, first with the bi-directional scheme and then with two uni-directional dry deposition schemes that have already been included in the model. The main objective of this study is to assess the performances of these three dry deposition schemes in atmospheric  $\text{NH}_3$  modeling using a detailed data set of  $\text{NH}_3$  measurements. The uncertainties associated with using predefined emission potentials in the bi-directional scheme are also examined.

## 2 Model description

### 2.1 STILT-Chem for $\text{NH}_3$

STILT-Chem v0.8 was employed in this study to simulate emissions, transport, transformation, and deposition of atmospheric  $\text{NH}_3$  as well as other key atmospheric species. STILT-Chem (Wen et al., 2012, 2013) is a stochastic Lagrangian air quality model developed from the Stochastic Time-Inverted Lagrangian Transport model (STILT; see <http://www.stilt-model.org>) (Lin et al., 2003). A STILT-Chem simulation begins with a stochastic back-trajectory simulation, followed by forward calculations that determine tracer concentrations along the generated back trajectories. In the back-trajectory simulation, numerous virtual particles, each representing an air parcel, are released from a receptor and transported backward in time for a specific period. Each particle is transported by both interpolated mean wind fields as well as stochastic velocities representing turbulent eddies. After back trajectories have been calculated, the concentrations of modeled species are initialized at the endpoint of each back trajectory using values output from a global chemical transport model. The initial parcel concentrations are then evolved forward in time along each trajectory to take into consideration the influences

## An evaluation of different dry deposition schemes

D. Wen et al.

Title Page

Abstract

Introduction

Conclusions

References

Tables

Figures

⏪

⏩

◀

▶

Back

Close

Full Screen / Esc

Printer-friendly Version

Interactive Discussion



of emissions, deposition, and chemical transformation. STILT-Chem uses the Carbon Bond IV (CB4) gas-phase chemical mechanism (Gery et al., 1989) to simulate the time evolution of the concentration of a variety of gas-phase species in the atmosphere while using an additional chemistry module to simulate the multiphase species involved in the key atmospheric reactions of atmospheric  $\text{NH}_3$  and ammonium. A comprehensive description of the treatment of emission, transport, transformation, and deposition of atmospheric  $\text{NH}_3$  and ammonium in STILT-Chem can be found in Wen et al. (2013).

## 2.2 Two uni-directional dry deposition schemes

### 2.2.1 Wesely dry deposition scheme

A dry deposition scheme based on the work of Wesely (1989) (hereafter referred to as “WDD”) was used as the default in STILT-Chem to compute dry deposition velocities of the modeled gaseous and aerosol species (Draxler and Hess, 1997). The WDD scheme estimates the dry deposition velocity by utilizing the resistance analogy method (Fig. 1), in which each species-specific dry deposition velocity ( $v_d$  in  $\text{m s}^{-1}$ ) is calculated as (Draxler and Hess, 1997)

$$v_d = (R_a + R_b + R_c + R_a R_b v_g)^{-1} + v_g \quad (1)$$

where  $R_a$  ( $\text{m s}^{-1}$ ) is the aerodynamic resistance between a specified height and the surface,  $R_b$  ( $\text{m s}^{-1}$ ) is the quasi-laminar sublayer resistance, and  $R_c$  ( $\text{m s}^{-1}$ ) is the bulk canopy surface resistance and is zero for particles.  $R_a$  ( $\text{m s}^{-1}$ ) is computed using the friction velocity and the Businger stability functions for the surface layer;  $R_b$  ( $\text{m s}^{-1}$ ) is computed in different ways over land and sea: over the land, it is parameterized through the friction velocity and the diffusivity characteristics of the gas and over the sea it is assumed to be small and only limited by the atmospheric resistance (Slinn and Slinn, 1980; Wesely, 1989; Draxler and Hess, 1997).  $v_g$  ( $\text{m s}^{-1}$ ), gravitational settling velocity

for particles, is calculated as (Van der Hoven, 1968),

$$v_g = d_p^2 g (\rho_g - \rho) (18\mu)^{-1} \quad (2)$$

where  $d_p$  (m) is the particle diameter,  $g$  is the gravity of Earth ( $9.801 \text{ ms}^{-2}$ ),  $\rho$  ( $\text{gm}^{-3}$ ) is air density,  $\rho_g$  ( $\text{gm}^{-3}$ ) is particle density, and  $\mu$  is the dynamic viscosity of air ( $0.01789 \text{ gm}^{-1} \text{ s}^{-1}$ ). Note that  $v_g$  is zero for gases.

$R_c$  depends primarily upon a number of plant physiological and ground surface characteristics and is parameterized as (Wesely, 1989)

$$R_c = [1/(R_{st} + R_m) + 1/R_{cut} + 1/(R_{dc} + R_{cl}) + 1/(R_{ac} + R_g)]^{-1} \quad (3)$$

where  $R_{st}$  ( $\text{sm}^{-1}$ ) is the stomatal resistance,  $R_m$  ( $\text{sm}^{-1}$ ) is the mesophyll resistance,  $R_{cut}$  ( $\text{sm}^{-1}$ ) is the upper-canopy leaf cuticle (lu) resistance,  $R_{dc}$  is the resistance to gas-phase transfer by convection,  $R_{cl}$  ( $\text{sm}^{-1}$ ) is the lower canopy resistance,  $R_{ac}$  ( $\text{sm}^{-1}$ ) is the canopy height and density factor resistance, and  $R_g$  ( $\text{sm}^{-1}$ ) is the ground surface resistance.  $R_{st}$  is parameterized as

$$R_{st} = R_i D_{hx} [1 + (200/(G + 0.1))^2] [400/(T_s(40 - T_s))] \quad (4)$$

where  $R_i$  ( $\text{sm}^{-1}$ ) is the minimum resistance for water vapor, which depends upon season and land-cover,  $D_{hx}$  is the ratio of the diffusivity of water vapor to that of the pollutant,  $G$  ( $\text{Wm}^{-2}$ ) is the solar radiation reaching at the canopy, and  $T_s$  ( $^{\circ}\text{C}$ ) is the surface air temperature in the canopy. For temperatures outside the  $0\text{--}40^{\circ}\text{C}$  temperature range,  $R_{st}$  is set to a very large value. The other resistances ( $R_m$ ,  $R_{cut}$ ,  $R_{dc}$ ,  $R_{cl}$ ,  $R_{ac}$ ,  $R_g$ ) depend primarily upon the effective (relative to  $\text{SO}_2$ ) Henry's constant and the specific reactivity of the pollutant. The parameterization of those resistances can be found in Draxler and Hess (1997).

## GMDD

6, 6075–6115, 2013

### An evaluation of different dry deposition schemes

D. Wen et al.

Title Page

Abstract

Introduction

Conclusions

References

Tables

Figures

◀

▶

◀

▶

Back

Close

Full Screen / Esc

Printer-friendly Version

Interactive Discussion



## 2.2.2 Zhang dry deposition scheme

Another dry deposition scheme, based on the work of Zhang et al. (2001, 2003) (hereafter referred to as “ZDD”), has been added to STILT-Chem from version 0.7 as another option to calculate dry deposition of modeled gaseous and aerosol species (Wen et al., 2013). The ZDD scheme (Fig. 1) employs a methodology similar to the WDD scheme; however, it includes an improved representation of a number of non-stomatal resistances, including in-canopy aerodynamic ( $R_{ac}$ ), soil ( $R_g$ ), and cuticle resistances ( $R_{cut}$ ). Instead of using a constant non-stomatal resistance for a particular season and land type, ZDD calculates non-stomatal resistance for two archetypal gas-phase species,  $SO_2$  and  $O_3$ , as a function of friction velocity, relative humidity, and canopy wetness, as well as biological factors, such as canopy type, leaf area index (LAI), and growing period. Non-stomatal resistances for other species are scaled as a weighted average to those of  $SO_2$  and  $O_3$  based on similarities or differences of their chemical and physical characteristics. Other improvements of the ZDD scheme include a more realistic treatment of cuticle and ground resistance in winter and the specification of seasonally-dependent input parameters, including LAI, roughness length and resistance components (Zhang et al., 2003). The ZDD scheme, which is formulated for 26 land-use categories, can calculate dry deposition velocities for more than 30 gaseous species and 14 particulate species that are usually considered in regional air quality models. It has been widely used in air quality models (e.g., Zhang et al., 2002; Alexander et al., 2005; Nopmongcol et al., 2012).

## 2.3 Bi-directional $NH_3$ air-surface exchange scheme

In order to simulate bi-directional exchange of  $NH_3$  between the atmosphere and the Earth’s surface, a bi-directional air-surface exchange scheme developed by Zhang et al. (2010) (hereafter referred to as “ZBE”) was implemented into STILT-Chem v0.8 in this study. The ZBE scheme (see Fig. 1) was developed for application in region-scale air quality models, in which stomatal and soil emission potentials are specified

GMDD

6, 6075–6115, 2013

### An evaluation of different dry deposition schemes

D. Wen et al.

Title Page

Abstract

Introduction

Conclusions

References

Tables

Figures

⏪

⏩

◀

▶

Back

Close

Full Screen / Esc

Printer-friendly Version

Interactive Discussion



according to land-use category and season based on an extensive review of measurement and model studies.

In this scheme, the overall vertical flux  $F_t$  ( $\mu\text{g m}^{-2} \text{s}^{-1}$ ) at a reference height above the canopy can be calculated as

$$F_t = -\frac{(\chi_a - \chi_c)}{(R_a + R_b)} \quad (5)$$

where  $\chi_a$  ( $\mu\text{g m}^{-3}$ ) is the  $\text{NH}_3$  air concentration at the reference height, and  $\chi_c$  ( $\mu\text{g m}^{-3}$ ) is the  $\text{NH}_3$  air concentration at the canopy top and can be calculated as

$$\chi_c = \left( \frac{\chi_a}{R_a + R_b} + \frac{\chi_{st}}{R_{st} + R_m} + \frac{\chi_g}{R_{ac} + R_g} \right) \cdot \left( \frac{1}{R_a + R_b} + \frac{1}{R_{st} + R_m} + \frac{1}{R_{ac} + R_g} + \frac{1}{R_{cut}} \right)^{-1} \quad (6)$$

where  $\chi_{st}$  ( $\mu\text{g m}^{-3}$ ) is stomatal compensation point.  $\chi_g$  ( $\mu\text{g m}^{-3}$ ) is the soil compensation point. The same formulas used in the ZDD scheme are used in the ZBE scheme to calculate all resistances in Eq. (6). All those formulas can be found in the work of Zhang et al. (2003).

$\chi_{st}$  is defined chemically as the concentration at which there is both a thermodynamic equilibrium between  $\text{NH}_3$  in the liquid and gas phase and an acid-base equilibrium between  $\text{NH}_4^+$  and  $\text{NH}_3$  in the liquid phase.  $\chi_{st}$  can be either measured or calculated according to the formula (Nemitz et al., 2004)

$$\chi_{st} = 1.703 \times 10^{10} \left( \frac{161500}{T_{st}} \right) \exp \left( -\frac{10378}{T_{st}} \right) \Gamma_{st} \quad (7)$$

**An evaluation of different dry deposition schemes**

D. Wen et al.

Title Page	
Abstract	Introduction
Conclusions	References
Tables	Figures
⏪	⏩
◀	▶
Back	Close
Full Screen / Esc	
Printer-friendly Version	
Interactive Discussion	



where  $T_{st}$  (K) is the temperature of the leaf stomata and  $\Gamma_{st}$  is the stomatal emission potential at 1 atmosphere, and is given by the expression (Nemitz et al., 2000)

$$\Gamma_{st} = \frac{[\text{NH}_4^+]_{st}}{[\text{H}^+]_{st}} \quad (8)$$

5 where  $[\text{NH}_4^+]_{st}$  is the concentration of  $\text{NH}_4^+$  ( $\text{molL}^{-1}$ ) in the apoplastic fluid (fluid in a tissue level compartment formed by the continuum of cell walls of adjacent cells as well as the extracellular spaces).  $[\text{H}^+]_{st} = 10^{-\text{pH}}$  is the stomatal concentration of  $\text{H}^+$  ( $\text{molL}^{-1}$ ) with the pH of the intercellular fluid at 1 atmosphere.

Similarly,  $\chi_g$  is calculated (Nemitz et al., 2004) using the formulas

$$10 \quad \chi_g = 1.703 \times 10^{10} \left( \frac{161500}{T_g} \right) \exp \left( -\frac{10378}{T_g} \right) \Gamma_g \quad (9)$$

$$\Gamma_g = \frac{[\text{NH}_4^+]_g}{[\text{H}^+]_g} \quad (10)$$

15 where  $T_g$  (K) is the temperature of the ground surface,  $\Gamma_{st}$  is the stomatal emission potential, and  $[\text{NH}_4^+]_g$  and  $[\text{H}^+]_g$  are the concentrations of  $\text{NH}_4^+$  and  $\text{H}^+$  ( $\text{molL}^{-1}$ ) in the ground cover.

In the ZBE scheme, a set of stomatal ( $\Gamma_{st}$ ) and ground ( $\Gamma_g$ ) emission potentials are specified (Table 1) as inputs for each land-use category using empirically-derived values to generate  $\chi_{st}$  and  $\chi_g$  using Eqs. (7) and (9), respectively. This approach is especially useful for regional-scale air quality models because those values are generally not measured at regional scales and are not explicitly calculated in regional-scale models. These values are based on an extensive review of model and measurement studies. As a result, they are generally representative of emission potentials for each land use category and season. For forests and grasslands, two sets of  $\Gamma_{st}$  and  $\Gamma_g$  values are provided for the same land-use category to reflect different nitrogen contents

**An evaluation of different dry deposition schemes**

D. Wen et al.

Title Page	
Abstract	Introduction
Conclusions	References
Tables	Figures
◀	▶
◀	▶
Back	Close
Full Screen / Esc	
Printer-friendly Version	
Interactive Discussion	



– one for high-N canopies and the other for low-N canopies. For the atmospheric NH<sub>3</sub> modeling studies in which anthropogenic NH<sub>3</sub> emissions are used as an external input, following Eq. (6) the air concentration of NH<sub>3</sub> at the canopy top  $\chi_c$  can be calculated as (Trebs et al., 2006)

$$\chi_c = \left( \frac{\chi_a}{R_a + R_b} + \frac{\chi_{st}}{R_{st} + R_m} + \frac{\chi_g}{R_{ac} + R_g} + F_e \right) \cdot \left( \frac{1}{R_a + R_b} + \frac{1}{R_{st} + R_m} + \frac{1}{R_{ac} + R_g} + \frac{1}{R_{cut}} \right)^{-1} \quad (11)$$

where  $F_e$  ( $\mu\text{g m}^{-2} \text{s}^{-1}$ ) is the NH<sub>3</sub> anthropogenic emission flux from external inputs.

### 3 Model simulations

#### 3.1 Measurements used for simulation and comparison

Detailed measurements of NH<sub>3</sub> were carried out during the Southern Ontario Ammonia Passive Sampler Survey (SOAPSS), which ran from 4 April 2006 to 27 March 2007 (Vet et al., 2008). The objective of SOAPSS was to measure ambient concentrations of NH<sub>3</sub> at approximately 79 sites, mainly located in southern Ontario but also at a small number of Canadian sites outside of Ontario and US sites bordering the Great Lakes. The survey provided highly spatially-resolved atmospheric NH<sub>3</sub> concentration data, with distances between sites in southern Ontario of approximately 20 km. The NH<sub>3</sub> measurements were made using passive samplers and represent an integrated average of the near-surface NH<sub>3</sub> concentration over a one-week (before December 2006) or two-week (after November 2006) period. Out of all sites, 53 were selected as receptors and test sites in this study (Fig. 2), consisting of 39 agricultural sites and 14 forest sites. The other 26 sites, which were very close to transitions from one land-use type to

## An evaluation of different dry deposition schemes

D. Wen et al.

Title Page

Abstract

Introduction

Conclusions

References

Tables

Figures

◀

▶

◀

▶

Back

Close

Full Screen / Esc

Printer-friendly Version

Interactive Discussion



another, were not used in this study because their land-use types cannot be assigned with certainty at the model grid scale due to insufficient resolution of the meteorological input.

### 3.2 Simulation setup

STILT-Chem v0.8 was used to simulate hourly  $\text{NH}_3$  concentrations at the 53 sites (Fig. 2) for a period from 1 June to 30 November 2006. The model was driven by Eta Data Assimilation System (EDAS) data that were obtained from NOAA's Air Resources Laboratory (ARL) meteorological data archives. The EDAS data cover most of North America using  $185 \times 129$  grid cells with a horizontal spacing of 40 km and 26 vertical layers and are available at 3 hourly intervals. In the model simulations, ensembles of 500 particles were released every hour from each site location at a height of 5 m above ground. A particle ensemble size of 500 was shown in a previous study (Wen et al., 2013), using the same model and similar inputs, to be sufficient to achieve adequate accuracy while not considerably increasing the computational cost. The paths of those particles were followed backward in time for six days, which usually allowed them to travel far away from any sources near the receptors. The calculated back-trajectories were 3-dimensional and their vertical motions were calculated directly using vertical velocity fields in the input meteorological data. The size of the integration time steps for the back-trajectory calculations varied with time and location from 1 min to 1 h and were computed based on the requirement that the advection distance per time-step should be less than the grid spacing (Courant–Friedrichs–Lewy condition). The same time steps were then also used in the forward simulation for deposition and chemistry calculations.

Identical emissions and initial/boundary conditions to those described in Wen et al. (2013) were employed in this study. A detailed description of the emissions and initial/boundary conditions can be found in Wen et al. (2013). Concentrations of modeled species were initialized at the endpoints of trajectories using output from the Model for OZone And Related chemical Tracers, version 4 (MOZART-4) (Emmons et al., 2010),

## An evaluation of different dry deposition schemes

D. Wen et al.

Title Page

Abstract

Introduction

Conclusions

References

Tables

Figures



Back

Close

Full Screen / Esc

Printer-friendly Version

Interactive Discussion



## An evaluation of different dry deposition schemes

D. Wen et al.

Title Page

Abstract

Introduction

Conclusions

References

Tables

Figures

⏪

⏩

◀

▶

Back

Close

Full Screen / Esc

Printer-friendly Version

Interactive Discussion

which was obtained from the WRF-Chem website (<http://www.acd.ucar.edu/wrf-chem/mozart.shtml>). The gridded MOZART-4 output fields have a  $2.8^\circ \times 2.8^\circ$  horizontal grid spacing with 28 vertical levels from the surface to approximately 2 hPa in six-hourly intervals. No interpolation of the output was performed for the particle initialization. MOZART-4 chemical species were mapped onto CB4 species according to the matching table given by Emmons et al. (2010). The initial concentrations of particles at trajectory endpoints were then evolved forward in time to account for the influences of emissions, chemical reactions and deposition along each trajectory for each time step in the forward trajectory integrations.

The 2006 Canadian Criteria Air Contaminants emission inventory (version 2) from Environment Canada (EC) was employed as the Canadian emission inventory in the simulations, which incorporates facility-level emissions from the EC National Pollutant Release Inventory plus province level estimates of on-road mobile emissions, off-road mobile emissions, and area emissions (<http://www.ec.gc.ca/inrp-npri/>). A special inventory of 2006 Canadian agricultural  $\text{NH}_3$  emissions that was developed under the Canadian National Agri-Environmental Standards Initiative (NAESI) was also included (Makar et al., 2009) to represent regional differences in farming practices and climatic conditions for each livestock category, and temporal variation due to seasonally varying agricultural practices or temperatures. The corresponding US and Mexican emissions inventories were the 2005 US National Emissions Inventory (version 4) and the 1999 Mexican emissions inventory. Both were obtained from the US Environmental Protection Agency (<http://www.epa.gov/ttn/chief/eiinformation.html>). These three national anthropogenic inventories all included emissions of oxides of nitrogen ( $\text{NO}_x$ ), VOC,  $\text{NH}_3$ , carbon monoxide (CO), oxides of sulphur ( $\text{SO}_x$ ), and primary particulate matter (PM) with an aerodynamic diameter less than or equal to  $10 \mu\text{m}$  and  $2.5 \mu\text{m}$  ( $\text{PM}_{10}$  and  $\text{PM}_{2.5}$ ). Each of the three national emissions inventories was processed by the Sparse Matrix Operator Kernel Emission (SMOKE) (v2.4) (UNC, 2009) emissions processing system for a domain (Fig. 2) that consisted of  $150 \times 106$  grid cells with a horizontal grid spacing of 42 km on a secant-polar-stereographic map projection

## An evaluation of different dry deposition schemes

D. Wen et al.

Title Page

Abstract

Introduction

Conclusions

References

Tables

Figures

⏪

⏩

◀

▶

Back

Close

Full Screen / Esc

Printer-friendly Version

Interactive Discussion



true at 60° N. The SMOKE-processed output emissions consisted of hourly gridded emissions fields that accounted for geographic variations and diurnal, weekly and monthly variations. For simplicity all point sources were treated as surface sources, which is reasonable for NH<sub>3</sub> emissions because all point sources account for a small fraction of total NH<sub>3</sub> emission ([http://www.ec.gc.ca/inrp-npri/default.asp?lang=en&n=0EC58C98-1#Emission\\_Summaries](http://www.ec.gc.ca/inrp-npri/default.asp?lang=en&n=0EC58C98-1#Emission_Summaries)).

Three dry deposition schemes, including two uni-directional schemes – ZDD and WDD – and the bi-directional scheme ZBE, were used in different STILT-Chem simulations for the 1 June to 30 November 2006 period to investigate their impacts on model predictions of NH<sub>3</sub> ambient concentrations. In the ZBE scheme, as mentioned above (Sect. 2.3), two sets of  $\Gamma_{st}$  and  $\Gamma_g$  values are available for the same land-use category for forests and grasslands according to canopy nitrogen content. Zhang et al. (2010) suggested that the higher values should be chosen for high-N canopies and the lower values should be chosen for low-N canopies. The classification of high-N and low-N canopy for each model grid cell can be determined according to a total nitrogen deposition map for the model domain obtained either from measurements or previous mode runs. In this study, due to a lack of such N deposition maps, we assumed low-N canopies for all forests and grasslands. This assumption appears to be reasonable because forest areas near the southern Ontario test sites have low NH<sub>3</sub> emission strengths and concentrations (cf. Figs. 2 and 3); thus N deposition in those forest areas should be low because NH<sub>3</sub> tends to be a local pollutant. Accordingly, in the STILT-Chem simulation with the ZBE scheme, the minimum emission potential values listed in Table 1 were used and the simulation was treated as a base-case simulation. However, the difference in the modeled NH<sub>3</sub> concentrations between simulations by assuming low-N canopies and by assuming High-N canopies for all forests and grasslands were examined. Some sensitivity simulations were also performed in which larger emission potential values were used for agricultural land-use categories in the ZBE scheme (see Sect. 4.3).

## 4 Results

### 4.1 Measured and modeled NH<sub>3</sub> concentrations using different dry deposition schemes

Figure 3 shows a site-by-site comparison of average NH<sub>3</sub> concentrations between simulations and observations, in which hourly modeled and weekly observed NH<sub>3</sub> concentrations were averaged over the entire simulation period from 1 June to 30 November 2006 for each site for the three simulations that used each of the three deposition schemes. Based on the good agreement obtained between simulated and observed values for a similar simulation (Wen et al., 2013), we assumed that the NH<sub>3</sub> emission inventory used in this study is reasonable and that the physical and chemical processes (other than dry deposition schemes) do not bias NH<sub>3</sub> concentration systematically over the regional scale, so that differences in the modeled NH<sub>3</sub> concentration from using the three dry deposition schemes can be compared. Note again that minimum values of stomatal emission potentials and ground emission potentials given in Table 1 were used in the simulation using the ZBE scheme. We can see from Fig. 3 that the STILT-Chem model using all three schemes generally performed adequately in predicting the average levels of observations for most sites, and also performed well in capturing the general transitional trend in the observations going from forested regions to agricultural regions (see Fig. 2). This is a positive result considering the fact that NH<sub>3</sub> is generally difficult for air quality models to simulate due to its strong spatial variability. Although STILT-Chem is based on Lagrangian reference framework and capable to capture sub-grid-scale variability (Wen et al., 2011), some processes such as emissions are associated with Eulerian grids in the simulation, and thus the model's performance is still affected by the resolution of input. Overall, out of the three schemes, NH<sub>3</sub> concentrations predicted using the ZDD scheme were smallest mainly because this scheme generally gives higher NH<sub>3</sub> dry deposition velocities (see Sect. 4.2). The highest NH<sub>3</sub> concentrations were predicted by the ZBE scheme due mainly to the inclusion of additional NH<sub>3</sub> emissions from ground and canopy vegetation.



using values of the mean time series displayed in Fig. 5, the ZDD scheme performed best in capturing average levels of observation for forest sites, with a Ratio Of the Means (ROM, defined in Table 2) of 0.97, compared with 1.30 for WDD and 1.71 for ZBE, respectively. The ZBE scheme, on the other hand, performed best in capturing average levels for both agricultural sites and all sites. For agricultural sites ZBE had a ROM of 1.04, compared 0.73 for ZDD and 0.83 for WDD, and for all sites the ZBE scheme had a ROM of 1.07, compared with 0.74 for ZDD and 0.85 for WDD. All three schemes had relatively poor correlations with observations for all three groups of sites, with a maximum value of 0.48. The ZBE scheme obviously overestimated  $\text{NH}_3$  concentrations over forest sites in terms of average observed concentration, and the ZDD scheme greatly underestimated  $\text{NH}_3$  concentrations over agricultural sites. The time series show a sharp decrease in modeled  $\text{NH}_3$  concentrations (especially at agricultural sites) for all three schemes after mid-October in response to decrease in the estimated  $\text{NH}_3$  emissions. After October, emissions of  $\text{NH}_3$  from livestock production in southern Ontario are expected to decrease, and fertilizer application was generally negligible in the winter months (Lillyman et al., 2009). In addition, snow cover in southern Ontario typically begins in November, substantially reducing  $\text{NH}_3$  soil emissions. A big difference between modeled and observed  $\text{NH}_3$  concentrations, however, may suggest that the decrease in the  $\text{NH}_3$  emissions after October was probably overestimated.

To further evaluate the performance of the three schemes, we calculated normalized standard deviations (NSD), centered normalized root-mean-squares (NRMS) and correlations ( $R$ ) (see Table 2 and Table 3) of weekly modeled  $\text{NH}_3$  concentrations against observations for the forest sites, the agricultural sites, and all test sites, respectively. Values of these three calculated statistics are shown graphically for the three schemes in Fig. 6 as Taylor diagrams (Taylor, 2001), which provide a way of summarizing graphically how closely a pattern (or a set of patterns) matches observations. Simulated patterns that agree well with observations will lie closer to the reference point marked “observed” on the  $x$  axis in a Taylor diagram. From Fig. 6, we can see

## GMDD

6, 6075–6115, 2013

### An evaluation of different dry deposition schemes

D. Wen et al.

Title Page

Abstract

Introduction

Conclusions

References

Tables

Figures

⏪

⏩

◀

▶

Back

Close

Full Screen / Esc

Printer-friendly Version

Interactive Discussion



that the performances of all schemes did not differ substantially for agricultural sites and for all sites. The WDD scheme had the best performance for them, which is somewhat different from what is suggested by the MFB and MFE values in Table 3. The reason is that the means of the fields in the Taylor diagram are subtracted out before computing their second-order statistics, so the diagram does not provide information about overall biases, but solely characterizes the centered pattern error. The simulated patterns by all schemes agreed much better with the observations for all sites and for the agricultural sites than the forest sites. All three schemes performed poorly in capturing observed patterns for the forest sites, with bigger NRMS, NSD values and smaller correlations. Due to much lower emissions strengths and concentration levels, the same uncertainty in the simulations may lead to more pronounced error/bias in the modeled  $\text{NH}_3$  concentrations for the forest sites than for the agricultural sites. Figure 6 confirmed again that the ZDD scheme performed better than the other dry deposition schemes for the forest sites.

## 4.2 Modeled dry deposition velocity and flux using different schemes

Hourly modeled results for the entire simulation period were used to calculate average diurnal variations of  $\text{NH}_3$  concentration, dry deposition velocity and air/surface exchange flux. The resulting diurnal variations in these three quantities for the three schemes are presented in Fig. 7 for the forest sites and the agricultural sites. Figure 7 shows that the dry deposition velocities of  $\text{NH}_3$  modeled by the WDD scheme were smaller than those modeled by the ZDD scheme for both the agricultural and especially for the forest sites. The underestimation of dry deposition velocities by the WDD scheme has been reported by other studies (Wu et al., 2012) and was attributed to the use of a prescribed minimum non-stomatal resistance without consideration of key biological factors (e.g., LAI). In contrast, the non-stomatal resistance parameterizations adopted in the ZDD scheme vary with biological (LAI), meteorological (friction velocity, relative humidity), and surface (canopy wetness) conditions, and therefore are better able to capture the variations of dry deposition velocity than the simple

## An evaluation of different dry deposition schemes

D. Wen et al.

Title Page

Abstract

Introduction

Conclusions

References

Tables

Figures

⏪

⏩

◀

▶

Back

Close

Full Screen / Esc

Printer-friendly Version

Interactive Discussion



---

## An evaluation of different dry deposition schemes

D. Wen et al.

---

Title Page

Abstract

Introduction

Conclusions

References

Tables

Figures

⏪

⏩

◀

▶

Back

Close

Full Screen / Esc

Printer-friendly Version

Interactive Discussion



non-stomatal resistance parameterization in the WDD scheme. The  $\text{NH}_3$  dry deposition velocity estimated by WDD for forest sites was even smaller than that for the agricultural sites, mainly due to an infinite minimum canopy stomatal resistance assigned in the WDD scheme for the deciduous forest category in the “autumn” season. In WDD, September–October is treated as autumn and foliage loss is thus assumed. The underprediction of dry deposition velocities of  $\text{O}_3$  by the WDD scheme for September – October has also been reported (Wu et al., 2011). The ZBE scheme calculated  $\text{NH}_3$  flux directly and no  $\text{NH}_3$  dry deposition velocity was estimated in the ZBE scheme.

Modeled  $\text{NH}_3$  fluxes using ZDD and WDD show evident diurnal patterns in which absolute flux magnitudes were smaller at night and larger during daytime hours. All fluxes were negative (i.e., downward out of the atmosphere) due to consideration solely of dry deposition in those uni-directional schemes. Although modeled  $\text{NH}_3$  dry deposition velocities by ZDD were larger for forest sites than for agricultural sites,  $\text{NH}_3$  fluxes modeled by both WDD and ZDD were higher for agricultural sites than for forest sites. The main reason is that dry deposition flux is determined not only by dry deposition velocity but also by ambient concentration, and  $\text{NH}_3$  concentrations at the agricultural sites were much higher than those at the forest sites as shown in Fig. 7. Downward fluxes predicted by ZDD were greater than those by WDD for both forest and agricultural sites: as a consequence, modeled  $\text{NH}_3$  concentrations based on ZDD were generally smaller than those based on WDD (see also Figs. 3 and 5).

Unlike the diurnal patterns of  $\text{NH}_3$  surface fluxes predicted by the uni-directional schemes, in which all fluxes were downward (negative), the  $\text{NH}_3$  surface fluxes predicted by the ZBE scheme were mostly upward (positive), especially for the agricultural sites where almost all fluxes were positive and had a much higher peak. Estimated fluxes over the forest sites were negative at night (Fig. 7) but reached maximum (positive) values in the afternoon. Flux peaks for both the agricultural sites and the forest sites are coincident with the ambient concentration minima. The mean flux of the pattern was about  $-1.2 \text{ ng m}^{-2} \text{ s}^{-1}$  for the forest sites, and  $19.2 \text{ ng m}^{-2} \text{ s}^{-1}$  for the

agricultural sites, indicating that  $\text{NH}_3$  air/surface exchange at the agricultural sites acted as an important source of  $\text{NH}_3$  to the atmosphere during the study period.

### 4.3 Uncertainty associated with emission potentials in the ZBE scheme

As discussed in Sect. 2.3, two parameters are required to determine air/surface exchange of  $\text{NH}_3$ : stomatal emission potential ( $\Gamma_{\text{st}}$ ) and soil emission potential ( $\Gamma_{\text{g}}$ ). Although these parameters can be measured at selected locations, they are not available at regional scales nor are they calculated in regional-scale air quality models. For regional-scale air quality modeling applications, the ZBE scheme employs  $\Gamma_{\text{st}}$  and  $\Gamma_{\text{g}}$  values that have been derived empirically for each land-use category. Two empirical sets of  $\Gamma_{\text{st}}$  and  $\Gamma_{\text{g}}$  values were provided (Table 1) to reflect different nitrogen contents for the same land-use category that forests and grasslands might have. Thus the use of different empirical emission potential values could lead to different simulation results.

In order to bracket uncertainties in modeled  $\text{NH}_3$  concentrations associated with the use of the minimum and maximum emission-potential values, we ran the model twice – one using the minimum and the other using the maximum emission potentials given in Table 1 – with the ZBE scheme for every location in the simulation domain. Note that for some land use categories (e.g., crops) the same emission potential was used for both runs due to only one value being available. Modeled  $\text{NH}_3$  concentrations were then averaged over the entire simulation period for each test site, and the average concentrations for the two runs are presented in Fig. 8 for comparison. Figure 8 shows that differences in modeled  $\text{NH}_3$  concentrations from using the maximum and minimum emission potentials were marked, especially for most forest sites. The mean  $\text{NH}_3$  concentration for the forest sites was  $2.25 \mu\text{g m}^{-3}$  when maximum emission potentials were used, about four times the mean value of  $0.54 \mu\text{g m}^{-3}$  obtained when the minimum emission potentials were used. This result indicates the importance of using appropriate emission potentials in  $\text{NH}_3$  bi-directional modeling. Although the same emission potential values were used for both runs for agricultural locations (agriculture related land-use categories only had one emission-potential value: see Table 1),

## An evaluation of different dry deposition schemes

D. Wen et al.

Title Page

Abstract

Introduction

Conclusions

References

Tables

Figures

⏪

⏩

◀

▶

Back

Close

Full Screen / Esc

Printer-friendly Version

Interactive Discussion



differences in modeled concentrations for those locations were still evident. The mean  $\text{NH}_3$  concentration for agricultural sites was  $3.81 \mu\text{g m}^{-3}$ , approximately 1.5 times the mean concentration of  $2.42 \mu\text{g m}^{-3}$  obtained using minimum emission potentials. This difference probably resulted from the transport of higher  $\text{NH}_3$  concentrations from forest areas due to the use of maximum emission potentials.

Figure 9 shows relationships between deviations of modeled  $\text{NH}_3$  concentrations from observations and corresponding local mean anthropogenic  $\text{NH}_3$  emissions for each site (see Fig. 2). All data points in Fig. 9 are means for the entire simulation period and the modeled concentrations are from the simulation using the ZBE scheme with minimum emission potentials. It can be seen that the deviations of modeled  $\text{NH}_3$  concentrations from observed values were correlated with anthropogenic  $\text{NH}_3$  emissions. The model tended to overestimate  $\text{NH}_3$  concentrations for sites with low emissions while underestimating  $\text{NH}_3$  concentrations for sites with strong  $\text{NH}_3$  emissions. Figure 9 also shows that  $\text{NH}_3$  concentrations were generally underestimated for most sites where anthropogenic emission strengths were greater than  $6.0 \text{ moles s}^{-1} \text{ gridcell}^{-1}$ . The underestimation of  $\text{NH}_3$  concentrations at those sites indicates that emission potentials specified in the ZBE scheme (Table 1) might be not large enough. In order to quantify how much emission potentials might potentially be underestimated, we conducted several sensitivity tests using different emission potentials for all locations where mean anthropogenic  $\text{NH}_3$  emissions exceeded  $6.0 \text{ moles s}^{-1} \text{ gridcell}^{-1}$ . Out of 53 sites, there were five sites that satisfied this condition and they were all agricultural sites. Those five sites were selected as test sites in this sensitivity study. The values of emission potentials tested were 2, 3, 4, 6 times the magnitudes of the pre-defined values in Table 1 for land-use categories related to agriculture (categories 15 to 20 in Table 1). Note that those categories only have one emission-potential value for each category. Modeled mean  $\text{NH}_3$  concentrations over the entire simulation period were compared for these tests with observations and results are summarized in Table 4. Examination of Table 4 suggests that there is a strong sensitivity to the choice of emission potential value. It further suggests that the pre-defined values of the emission potentials used

## GMDD

6, 6075–6115, 2013

### An evaluation of different dry deposition schemes

D. Wen et al.

Title Page

Abstract

Introduction

Conclusions

References

Tables

Figures

⏪

⏩

◀

▶

Back

Close

Full Screen / Esc

Printer-friendly Version

Interactive Discussion



in the ZBE scheme might be substantially underestimated for sites with strong anthropogenic NH<sub>3</sub> emissions. According to these tests, values of emission potentials at least three times larger than those specified in Table 1 are required in order to reasonably predict NH<sub>3</sub> concentrations at sites with anthropogenic emission strengths greater than 6.0 ngm<sup>-2</sup>s<sup>-1</sup> gridcell<sup>-1</sup>.

## 5 Summary and conclusions

An air/surface bi-directional exchange scheme developed for regional NH<sub>3</sub> modeling was incorporated in STILT-Chem v0.8 for this study. STILT-Chem v0.8 was then applied to simulate NH<sub>3</sub> concentration at 53 measurement sites in southern Ontario for a simulation period from 1 June to 30 November 2006, using the bi-directional scheme (ZBE) and two uni-directional dry deposition schemes (WDD and ZDD). Modeled NH<sub>3</sub> concentrations using these three schemes were compared against weekly passive-sampler NH<sub>3</sub> measurements for each site. The comparisons indicate that all three schemes can generally reproduce the observed NH<sub>3</sub> concentrations reasonably well. However, the three schemes performed differently at locations with different concentration levels. Modeled results show that the bi-directional scheme performed best at locations with high observed NH<sub>3</sub> concentrations but overestimated NH<sub>3</sub> levels for locations with low observed NH<sub>3</sub> concentrations. The two uni-directional dry deposition schemes, on the other hand, performed better than the bi-directional scheme at sites with low observed NH<sub>3</sub> concentrations.

The absolute or relative errors in the modeled NH<sub>3</sub> concentrations from using the three different dry deposition schemes were examined and interpreted based on the assumption that other processes did not cause any systematic biases. One possible systematic bias, however, could be caused by the underestimation of NH<sub>3</sub> emissions as emissions data for biogeochemical sources like biogenic N fixation in agricultural systems and/or atmospheric deposition of NO<sub>y</sub> followed by soil N cycling processes (e.g., Beusen et al., 2008; Galloway et al., 2008) are generally not available and hence are

### An evaluation of different dry deposition schemes

D. Wen et al.

Title Page

Abstract

Introduction

Conclusions

References

Tables

Figures

◀

▶

◀

▶

Back

Close

Full Screen / Esc

Printer-friendly Version

Interactive Discussion



## An evaluation of different dry deposition schemes

D. Wen et al.

Title Page

Abstract

Introduction

Conclusions

References

Tables

Figures

⏪

⏩

◀

▶

Back

Close

Full Screen / Esc

Printer-friendly Version

Interactive Discussion



not included in available  $\text{NH}_3$  emissions inventories. The omission of such emissions could lead to underestimation of atmospheric  $\text{NH}_3$  concentrations. Although the appropriateness of this assumption cannot be verified directly in this study, the good agreement between model simulations and observations suggests that systematic biases in the simulations are small. Moreover, the absolute or relative errors caused by those systematic biases might be shifted to one direction only because the same model and input data were used for all three dry deposition schemes.

If stomatal and ground emission potentials were set to zero in the ZBE scheme, the ZBE scheme and the ZDD scheme would yield the same  $\text{NH}_3$  flux. The reason is that the ZBE scheme was developed from the ZDD scheme and both schemes uses the same formulas to compute the dry deposition component (Zhang et al., 2010). In other words, the ZDD scheme acts as a special case of the ZBE scheme in  $\text{NH}_3$  bi-directional exchange modeling. Since the ZDD scheme more accurately predicted  $\text{NH}_3$  concentrations at locations with low  $\text{NH}_3$  concentrations than the ZBE scheme (Fig. 4), the appropriateness of the application of the current version of the bi-directional scheme to low  $\text{NH}_3$  concentration locations needs reconsideration and further investigation. Uncertainties in the magnitudes of the emission-potential values used for both low-  $\text{NH}_3$  and high- $\text{NH}_3$  concentration locations also needs further investigation.

## 6 Code availability

STILT-Chem v0.8 is written in Fortran. The run of the model is controlled by a shell script. A brief manual is included in the model package. The code of the STILT-Chem v0.8 will be online for free access in the near future. For the time being, the model can be obtained by contacting John C. Lin (john.lin@utah.edu).

Supplementary material related to this article is available online at  
[http://www.geosci-model-dev-discuss.net/6/6075/2013/  
gmdd-6-6075-2013-supplement.pdf](http://www.geosci-model-dev-discuss.net/6/6075/2013/gmdd-6-6075-2013-supplement.pdf).

*Acknowledgements.* We gratefully acknowledge funding from Environment Canada for supporting D. Wen and the important contribution of G. Beaney of Environment Canada in making the SOAPSS ammonia measurements. We also thank Q. Zheng and J. Zhang of Environment Canada for preparing the emissions files used in this study. This work was made possible by the facilities of the Shared Hierarchical Academic Research Computing Network (SHARCNET: <http://www.sharcnet.ca>) and Compute/Calcul Canada.

## References

- Alexander, B., Park, R. J., Jacob, D. J., Li, Q. B., Yantosca, R. M., Savarino, J., Lee, C. C. W., and Thiemens, M. H.: Sulfate formation in sea-salt aerosols: constraints from oxygen isotopes, *J. Geophys. Res.*, 110, D10307, doi:10.1029/2004JD005659, 2005. 6081
- Bash, J. O., Cooter, E. J., Dennis, R. L., Walker, J. T., and Pleim, J. E.: Evaluation of a regional air-quality model with bidirectional NH<sub>3</sub> exchange coupled to an agroecosystem model, *Biogeosciences*, 10, 1635–1645, doi:10.5194/bg-10-1635-2013, 2013. 6077
- Beusen, A., Bouwman, A. F., Heuberger, P., Van Drecht, G., and Van Der Hoek, K. W.: Bottomup uncertainty estimates of global ammonia emissions from global agricultural production systems, *Atmos. Environ.*, 42, 6067–6077, doi:10.1016/j.atmosenv.2008.03.044, 2008. 6095
- Chang, J. S.: NAPAP Report 4, the regional acid deposition model and engineering model, Appendix E, in: *Acid Deposition: State of Science and Technology*, vol I, Emissions, Atmospheric Processes, and Deposition, US Government Printing Office, Washington, DC, 20402–9325, 1990.
- Cooter, E. J., Bash, J. O., Walker, J. T., Jones, M. R., and Robarge, W.: Estimation of NH<sub>3</sub> bi-directional flux from managed agricultural soils, *Atmos. Environ.*, 44, 2107–2115, doi:10.1016/j.atmosenv.2010.02.044, 2010. 6077

GMDD

6, 6075–6115, 2013

## An evaluation of different dry deposition schemes

D. Wen et al.

Title Page

Abstract

Introduction

Conclusions

References

Tables

Figures

⏪

⏩

◀

▶

Back

Close

Full Screen / Esc

Printer-friendly Version

Interactive Discussion





## An evaluation of different dry deposition schemes

D. Wen et al.

Title Page

Abstract

Introduction

Conclusions

References

Tables

Figures

⏪

⏩

◀

▶

Back

Close

Full Screen / Esc

Printer-friendly Version

Interactive Discussion

servations: the Stochastic Time-inverted Lagrangian Transport (STILT) model, *J. Geophys. Res.*, 108, 4493, doi:10.1029/2002JD003161, 2003. 6078

Makar, P. A., Moran, M. D., Zheng, Q., Cousineau, S., Sassi, M., Duhamel, A., Besner, M., Davignon, D., Crevier, L.-P., and Bouchet, V. S.: Modelling the impacts of ammonia emissions reductions on North American air quality, *Atmos. Chem. Phys.*, 9, 7183–7212, doi:10.5194/acp-9-7183-2009, 2009. 6086

Morris, J. T.: Effects of nitrogen loading on wetland ecosystems with particular reference to atmospheric deposition, *Annu. Rev. Ecol. Syst.*, 22, 257–279, doi:10.1146/annurev.es.22.110191.001353, 1991. 6077

Nemitz, E., Sutton, M. A., Schjoerring, J. K., Husted, S., and Wyers, G. P.: Resistance modelling of ammonia exchange over oilseed rape, *Agr. Forest Meteorol.*, 105, 405–425, doi:10.1016/S0168-1923(00)00206-9, 2000. 6083

Nemitz, E., Milford, C., and Sutton, M. A.: A two-layer canopy compensation point model for describing bi-directional biosphere-atmosphere exchange of ammonia, *Q. J. Roy. Meteor. Soc.*, 127, 815–833, doi:10.1002/qj.49712757306, 2001. 6077

Nemitz, E., Sutton, M. A., Wyers, G. P., and Jongejan, P. A. C.: Gas-particle interactions above a Dutch heathland: I. Surface exchange fluxes of  $\text{NH}_3$ ,  $\text{SO}_2$ ,  $\text{HNO}_3$  and  $\text{HCl}$ , *Atmos. Chem. Phys.*, 4, 989–1005, doi:10.5194/acp-4-989-2004, 2004. 6082, 6083

Nopmongkol, U., Koo, B., Tai, E., Jung, J., Piyachaturawat, P., Emery, C., Yarwood, G., Pirovano, G., Mitsakou, C., and Kallos, G.: Modeling Europe with CAMx for the Air Quality Model Evaluation International Initiative (AQMEII), *Atmos. Environ.*, 53, 177–185, doi:10.1016/j.atmosenv.2011.11.023, 2012. 6081

Pleim, J. E., Bash, J. O., Walker, J. T., and Cooter, E. J.: Development and evaluation of an ammonia bi-directional flux parametrization for air quality models, *J. Geophys. Res.-Atmos.*, 118, 3794–3806, doi:10.1002/jgrd.50262, 2013. 6077

Pope, C. A., Ezzati, M., and Dockery, D. W.: Fine-particulate air pollution and life expectancy in the US, *New Engl. J. Med.*, 360, 376–386, doi:10.1056/NEJMsa0805646, 2009. 6076

Seinfeld, J. H. and Pandis, S. N.: *Atmospheric Chemistry and Physics: From Air Pollution to Climate Change*, 2nd edn., J. Wiley, New York, 2006. 6076

Simpson, D., Benedictow, A., Berge, H., Bergström, R., Emberson, L. D., Fagerli, H., Flechard, C. R., Hayman, G. D., Gauss, M., Jonson, J. E., Jenkin, M. E., Nyíri, A., Richter, C., Semeena, V. S., Tsyro, S., Tuovinen, J.-P., Valdebenito, Á., and Wind, P.: The EMEP MSC-

## An evaluation of different dry deposition schemes

D. Wen et al.

Title Page

Abstract

Introduction

Conclusions

References

Tables

Figures

◀

▶

◀

▶

Back

Close

Full Screen / Esc

Printer-friendly Version

Interactive Discussion

W chemical transport model – technical description, *Atmos. Chem. Phys.*, 12, 7825–7865, doi:10.5194/acp-12-7825-2012, 2012. 6077

Slinn, S. A. and Slinn, W. G. N.: Predictions for particle deposition on natural waters, *Atmos. Environ.*, 14, 1013–1016, doi:10.1016/0004-6981(80)90032-3, 1980. 6079

5 Sutton, M. A., Burkhardt, J. K., Guerin, D., Nemitz, E., and Fowler, D.: Development of resistance models to describe measurements of bi-directional ammonia surface-atmosphere exchange, *Atmos. Environ.*, 32, 473–480, doi:10.1016/S1352-2310(97)00164-7, 1998. 6077

Taylor, K. E.: Summarizing multiple aspects of model performance in a single diagram, *J. Geophys. Res.*, 106, 7183–7192, doi:10.1029/2000JD900719, 2001. 6090

10 Trebs, I., Lara, L. L., Zeri, L. M. M., Gatti, L. V., Artaxo, P., Dlugi, R., Slanina, J., Andreae, M. O., and Meixner, F. X.: Dry and wet deposition of inorganic nitrogen compounds to a tropical pasture site (Rondônia, Brazil), *Atmos. Chem. Phys.*, 6, 447–469, doi:10.5194/acp-6-447-2006, 2006. 6084

UNC: SMOKE V2.4 User's Manual, available at: <http://www.cmascenter.org/smoke/documentation/2.4/html/> (last access: 25 December 2013), 2009. 6086

15 Van Bremen, N., Burrough, P. A., Velthorst, E. J., van Dobben, H. F., de Wit, T., Ridder, T. B., and Reijnders, H. F. R.: Soil acidification from atmospheric ammonium sulphate in forest canopy throughfall, *Nature*, 299, 548–550, doi:10.1038/299548a0, 1982. 6077

20 Van der Hoven, I.: Deposition of particles and gases, *Meteorology and Atomic Energy*, in: *Meteorology and Atomic Energy*, edited by: Slade, D., US Atomic Energy Commission, 202–208, 1968. 6080

Vet, R., Li, S.-M., Beaney, G., Belzer, W., Chan, E., Dann, T., Friesen, K., Hayden, K., Hou, A., Iqbal, S., Jones, K., Leithead, A., Liggio, J., Makar, P., Narayan, J., Ro, C.-U., Shaw, M., Sukloff, B., Vingarzan, R., and Qiu, W.: Characterization of ambient ammonia, PM and regional deposition across Canada, Chapter 6, in: *Environment Canada. The 2008 Canadian Atmospheric Assessment of Agricultural Ammonia*, Environment Canada, Gatineau, QC, Canada, 93–147, 2008. 6084

25 Vieno, M., Dore, A. J., Stevenson, D. S., Doherty, R., Heal, M. R., Reis, S., Hallsworth, S., Tarrason, L., Wind, P., Fowler, D., Simpson, D., and Sutton, M. A.: Modelling surface ozone during the 2003 heat-wave in the UK, *Atmos. Chem. Phys.*, 10, 7963–7978, doi:10.5194/acp-10-7963-2010, 2010. 6077

30



## An evaluation of different dry deposition schemes

D. Wen et al.

Title Page

Abstract

Introduction

Conclusions

References

Tables

Figures

◀

▶

◀

▶

Back

Close

Full Screen / Esc

Printer-friendly Version

Interactive Discussion



- Wen, D., Lin, J. C., Meng, F., Gbor, P. K., He, Z., and Sloan, J. J.: Quantitative assessment of upstream source influences on total gaseous mercury observations in Ontario, Canada, *Atmos. Chem. Phys.*, 11, 1405–1415, doi:10.5194/acp-11-1405-2011, 2011. 6088
- Wen, D., Lin, J. C., Millet, D. B., Stein, A. F., and Draxler, R. R.: A backward-time stochastic Lagrangian air quality model, *Atmos. Environ.*, 54, 373–386, doi:10.1016/j.atmosenv.2012.02.042, 2012. 6078
- Wen, D., Lin, J. C., Zhang, L., Vet, R., and Moran, M. D.: Modeling atmospheric ammonia and ammonium using a stochastic Lagrangian air quality model (STILT-Chem v0.7), *Geosci. Model Dev.*, 6, 327–344, doi:10.5194/gmd-6-327-2013, 2013. 6078, 6079, 6081, 6085, 6088
- Wesely, M. L.: Parameterization of surface resistance to gaseous dry deposition in regional-scale numerical models, *Atmos. Environ.*, 23, 1293–1304, doi:10.1016/0004-6981(89)90153-4, 1989. 6079, 6080
- Wichink Kruit, R. J., Schaap, M., Sauter, F. J., van Zanten, M. C., and van Pul, W. A. J.: Modelling the distribution of ammonia across Europe including bi-directional surface–atmosphere exchange, *Biogeosciences*, 9, 5261–5277, doi:10.5194/bg-9-5261-2012, 2012. 6077, 6089
- Wu, Y., Walker, J., Schwede, D., Peters-Lidard, C., Dennis, R., and Robarge, W.: A new model of bi-directional ammonia exchange between the atmosphere and biosphere: ammonia stomatal compensation point, *Agr. Forest Meteorol.*, 149, 263–280, doi:10.1016/j.agrformet.2008.08.012, 2009. 6077
- Wu, Z., Wang, X., Chen, F., Turnipseed, A. A., Guenther, A. B., Niyogi, D., Charusombat, U., Xia, B., Munger, J. W., and Alapaty, K.: Evaluating the calculated dry deposition velocities of reactive nitrogen oxides and ozone from two community models over a temperate deciduous forest, *Atmos. Environ.*, 45, 2663–2674, doi:10.1016/j.atmosenv.2011.02.063, 2011. 6092
- Wu, Z., Wang, X., Turnipseed, A. A., Chen, F., Zhang, L., Guenther, A. B., Karl, T., Huey, L. G., Niyogi, D., Xia, B., and Alapaty, K.: Evaluation and improvements of two community models in simulating dry deposition velocities for peroxyacetyl nitrate (PAN) over a coniferous forest, *J. Geophys. Res.-Atmos.*, 117, D04310, doi:10.1029/2011JD016751, 2012. 6091
- Zhang, L., Gong, S., Padro, J., and Barrie, L.: A size-segregated particle dry deposition scheme for an atmospheric aerosol module, *Atmos. Environ.*, 35, 549–560, doi:10.1016/S1352-2310(00)00326-5, 2001. 6081
- Zhang, L., Moran, M., Makar, P., Brook, J., and Gong, S.: Modelling gaseous dry deposition in AURAMS: a unified regional air-quality modelling system, *Atmos. Environ.*, 36, 537–560, doi:10.1016/S1352-2310(01)00447-2, 2002. 6081

Zhang, L., Brook, J. R., and Vet, R.: A revised parameterization for gaseous dry deposition in air-quality models, *Atmos. Chem. Phys.*, 3, 2067–2082, doi:10.5194/acp-3-2067-2003, 2003. 6081, 6082

5 Zhang, L., Wright, L. P., and Asman, W. A. H.: Bi-directional air-surface exchange of atmospheric ammonia: a review of measurements and a development of a big-leaf model for applications in regional-scale air-quality models, *J. Geophys. Res.*, 115, D20310, doi:10.1029/2009JD013589, 2010. 6077, 6078, 6081, 6087, 6096, 6103

## GMDD

6, 6075–6115, 2013

### An evaluation of different dry deposition schemes

D. Wen et al.

Title Page

Abstract

Introduction

Conclusions

References

Tables

Figures

⏪

⏩

◀

▶

Back

Close

Full Screen / Esc

Printer-friendly Version

Interactive Discussion





## An evaluation of different dry deposition schemes

D. Wen et al.

Title Page

Abstract

Introduction

Conclusions

References

Tables

Figures

⏪

⏩

◀

▶

Back

Close

Full Screen / Esc

Printer-friendly Version

Interactive Discussion



**Table 2.** Definition of statistical metrics.

Parameter	Definition
Ratio of the Means (ROM)	$\left(\frac{1}{N} \sum_{i=1}^N P_i\right) / \left(\frac{1}{N} \sum_{i=1}^N O_i\right)$
Mean Fractional Bias (MFB)	$\frac{1}{N} \sum_{i=1}^N \frac{P_i - O_i}{(P_i + O_i)/2} \times 100\%$
Mean Fractional Error (MFE)	$\frac{1}{N} \sum_{i=1}^N \frac{ P_i - O_i }{(P_i + O_i)/2} \times 100\%$
Standard Model Deviation ( $\sigma_p$ )	$\sqrt{\frac{1}{N} \sum_{i=1}^N (P_i - \bar{P})^2}$
Standard Observation Deviation ( $\sigma_o$ )	$\sqrt{\frac{1}{N} \sum_{i=1}^N (O_i - \bar{O})^2}$
Correlation ( $R$ )	$\left[ \frac{1}{N} \sum_{i=1}^N (P_i - \bar{P})(O_i - \bar{O}) \right] / (\sigma_p \sigma_o)$
Centered Normalized Root-Mean-Square (NRMS)	$\sqrt{\frac{1}{N} \sum_{i=1}^N [(P_i - \bar{P}) - (O_i - \bar{O})]^2 / \sigma_o^2}$
Normalized Standard Deviation (NSD)	$\sigma_p / \sigma_o$

$P_i$ : prediction at time  $i$ .

$O_i$ : observation at time  $i$ .

$N$ : total number of observations or predictions.

$\bar{P}$ : the overall mean of predictions.

$\bar{O}$ : the overall mean of observations.

## An evaluation of different dry deposition schemes

D. Wen et al.

Title Page

Abstract

Introduction

Conclusions

References

Tables

Figures

◀

▶

◀

▶

Back

Close

Full Screen / Esc

Printer-friendly Version

Interactive Discussion



**Table 3.** Values of six statistical metrics for comparison of weekly modeled  $\text{NH}_3$  concentrations against observations for the 1 June to 30 November 2006 period for three groups of sites: (1) all sites (53); (2) forested sites (14); (3) agricultural sites (39).

Metrics	All sites			Agricultural sites			Forested sites		
	WDD	ZDD	ZBE	WDD	ZDD	ZBE	WDD	ZDD	ZBE
ROM	0.85	0.74	1.07	0.83	0.73	1.04	1.27	0.95	1.68
MFB	-2.40	-24.18	23.40	-14.15	-26.48	12.72	32.77	-17.30	55.32
MFE	56.65	52.25	57.73	48.04	50.10	49.38	82.37	58.66	82.72
R	0.60	0.62	0.55	0.49	0.51	0.40	0.05	0.05	0.27
NSD	0.43	0.34	0.50	0.39	0.30	0.40	1.78	1.03	2.56
NRMS	0.79	0.80	0.85	0.86	0.88	0.92	1.99	1.39	2.48

## An evaluation of different dry deposition schemes

D. Wen et al.

Title Page

Abstract

Introduction

Conclusions

References

Tables

Figures

◀

▶

◀

▶

Back

Close

Full Screen / Esc

Printer-friendly Version

Interactive Discussion



**Table 4.** Selected statistics for emission-potential sensitivity tests with the ZBE scheme for five measurement sites with strong anthropogenic  $\text{NH}_3$  emissions. PEP is pre-defined emission-potential values in Table 1 for land-use categories related to agriculture.

Tested emission potentials	ROM	MFB (%)	MFE (%)
1 × PEP	0.79	−22.59	22.59
2 × PEP	0.88	−13.56	14.43
3 × PEP	0.99	−2.13	11.11
4 × PEP	1.09	8.15	11.31
6 × PEP	1.31	25.87	25.87

**An evaluation of different dry deposition schemes**

D. Wen et al.

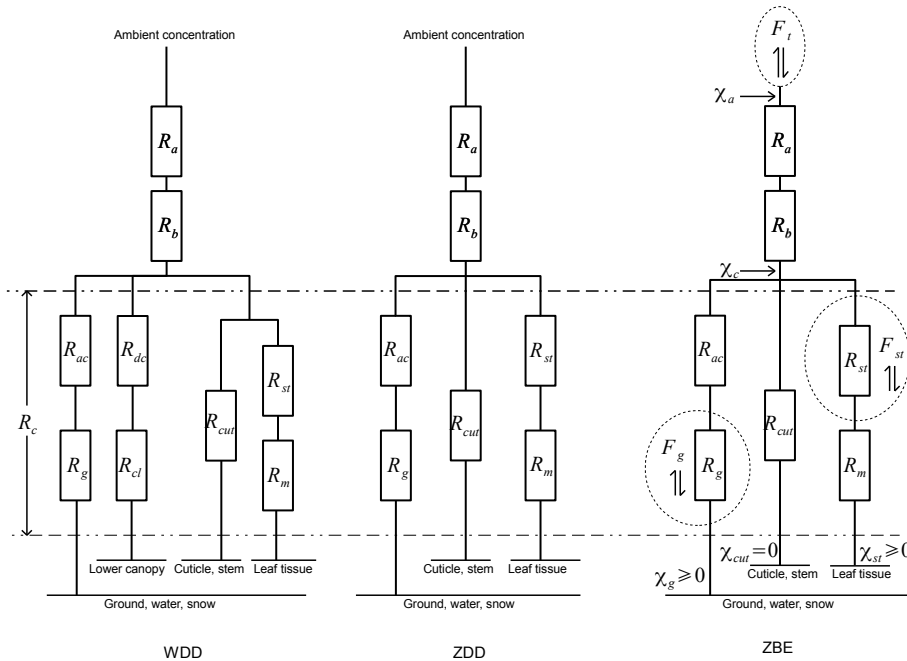


**Fig. 1.** Diagrammatic representation of the WDD, ZDD, and ZBE schemes. Resistances include the aerodynamic resistance ( $R_a$ ), the quasi-laminar sublayer resistance above the canopy ( $R_b$ ), and the overall canopy resistance ( $R_c$ ).  $R_c$  can be decomposed into stomatal resistance ( $R_{st}$ ), mesophyll resistance ( $R_m$ ), in-canopy aerodynamic resistance ( $R_{ac}$ ), soil resistance ( $R_g$ ), cuticle resistance ( $R_{cut}$ ), lower canopy resistance ( $R_{cl}$ ), and resistance for the gas transfer affected by buoyant convection in the canopy ( $R_{dc}$ ).  $F_t$  is overall flux at a reference height above the canopy.  $F_{st}$  and  $F_g$  are bi-directional fluxes through stomata and above the soil surface, respectively.  $\chi_a$  is the ambient concentration at the reference height.  $\chi_c$  is the concentration at the top of canopy.  $\chi_{st}$  and  $\chi_g$  are the stomatal and soil compensation points, respectively.

Title Page

Abstract Introduction

Conclusions References

Tables Figures

◀ ▶

◀ ▶

Back Close

Full Screen / Esc

Printer-friendly Version

Interactive Discussion



An evaluation of  
different dry  
deposition schemes

D. Wen et al.

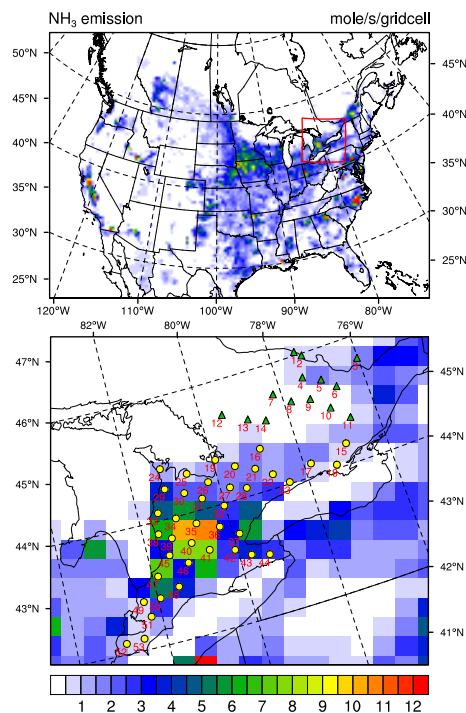


**Fig. 2.** Locations of IDs of 53 measurement sites and spatial distribution of gridded  $\text{NH}_3$  emissions fluxes ( $\text{mol s}^{-1} \text{ grid cell}^{-1}$ ) over the simulation domain (top panel) and their local  $\text{NH}_3$  emission fluxes (bottom panel is a magnification of the area enclosed by red lines in the top panel). Measurement sites include 14 forest sites (green triangles) and 39 agricultural sites (yellow dots). Note that the emission fluxes are averages over the entire simulation period.

## An evaluation of different dry deposition schemes

D. Wen et al.

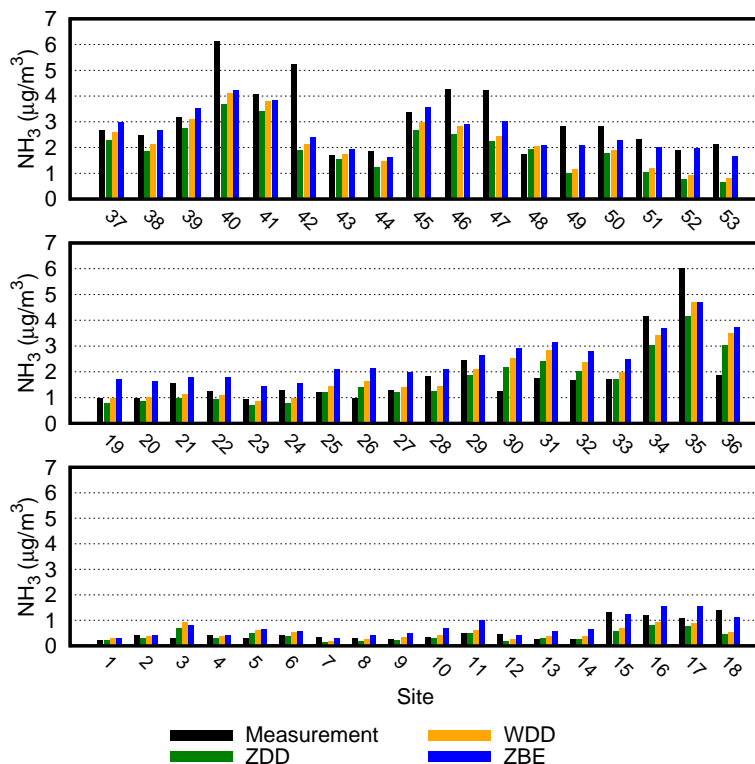


**Fig. 3.** Observed (black) and modeled  $\text{NH}_3$  concentration averages with the WDD scheme (orange), the ZDD scheme (green), and the ZBE scheme (blue) for 53 measurement sites for the 1 June to 30 November 2006 period. Sites 1 to 14 are forest sites.

Title Page

Abstract Introduction

Conclusions References

Tables Figures

◀ ▶

◀ ▶

Back Close

Full Screen / Esc

Printer-friendly Version

Interactive Discussion



## An evaluation of different dry deposition schemes

D. Wen et al.

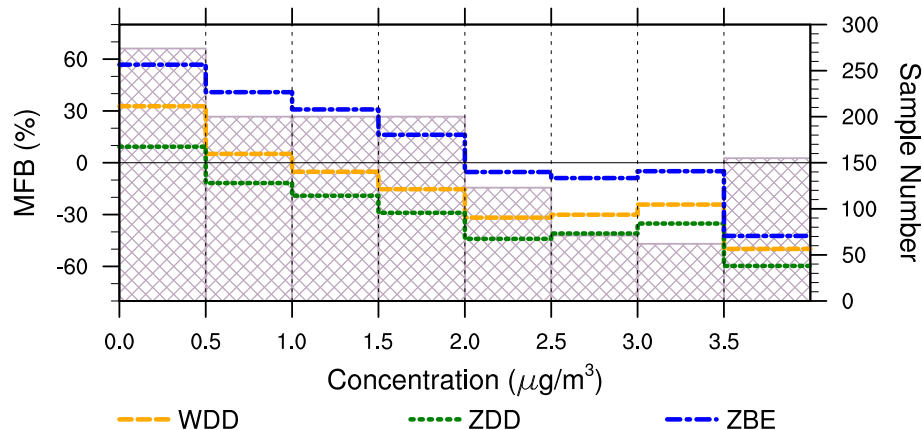


**Fig. 4.** Mean fractional bias (left axis) of weekly modeled  $\text{NH}_3$  concentrations against observations for eight different observed  $\text{NH}_3$  concentration ranges for the 1 June to 30 November 2006 period. The modeled  $\text{NH}_3$  concentrations are simulation results for all 53 sites using the WDD (orange), ZDD (green), and ZBE (blue) schemes, respectively. Cross-hatched bars (right axis) show the number of data points in each concentration range.

Title Page

Abstract

Introduction

Conclusions

References

Tables

Figures

◀

▶

◀

▶

Back

Close

Full Screen / Esc

Printer-friendly Version

Interactive Discussion



## An evaluation of different dry deposition schemes

D. Wen et al.

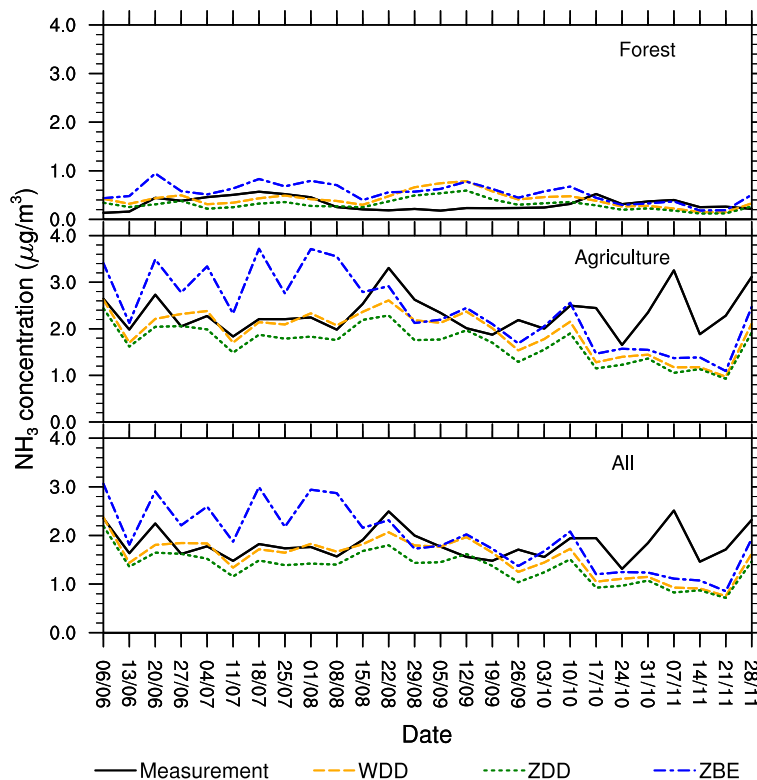


**Fig. 5.** Observed  $\text{NH}_3$  concentration time series (black continuous line) vs. modeled time series using the WDD scheme (orange), the ZDD scheme (green), and the ZBE scheme (blue), respectively. Those time series are averages over forest sites (top), agricultural sites (middle), and all 53 sites (bottom).

Title Page

Abstract

Introduction

Conclusions

References

Tables

Figures

◀

▶

◀

▶

Back

Close

Full Screen / Esc

Printer-friendly Version

Interactive Discussion



## An evaluation of different dry deposition schemes

D. Wen et al.

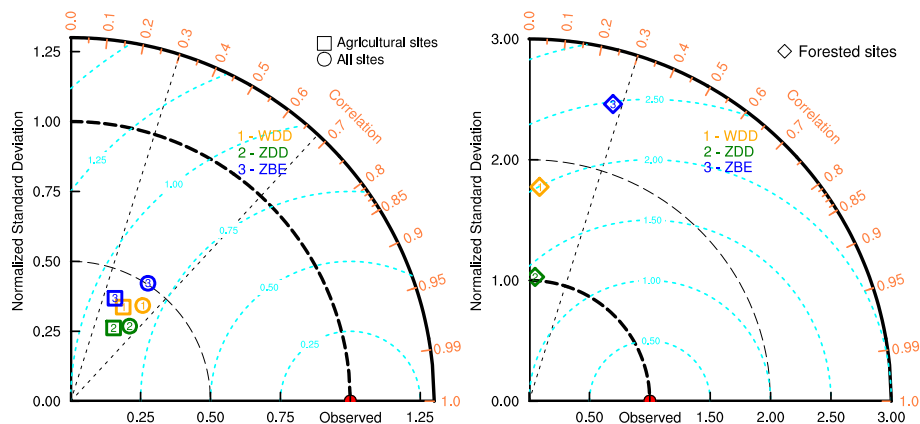


**Fig. 6.** Taylor diagrams displaying normalized standard deviations (NSD (black dashed curve)), centered normalized root-mean-squares (NRMS (cyan dashed curve)) and correlations ( $R$ ) of weekly modeled mean  $\text{NH}_3$  concentrations using WDD (orange), ZDD (green) and ZBE (blue) against observations (red dot) for three groups of sites: all test sites (circles, left panel), agricultural sites (squares, left panel), and forested sites (diamonds, right panel).

Title Page

Abstract Introduction

Conclusions References

Tables Figures

◀ ▶

◀ ▶

Back Close

Full Screen / Esc

Printer-friendly Version

Interactive Discussion



## An evaluation of different dry deposition schemes

D. Wen et al.

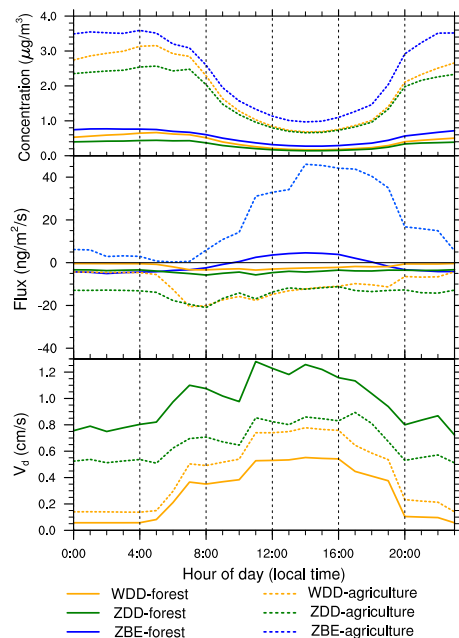


**Fig. 7.** Diurnal variations of modeled dry deposition velocity (bottom), surface exchange flux (middle), and  $\text{NH}_3$  concentration using WDD (orange), ZDD (green), and ZBE (blue) schemes respectively, averaged over the entire simulation period for forest sites (solid lines) and agricultural sites (dashed lines). Negative values represent downward fluxes out of the atmosphere whereas positive fluxes represent emission from surface to the atmosphere.

Title Page

Abstract

Introduction

Conclusions

References

Tables

Figures



Back

Close

Full Screen / Esc

Printer-friendly Version

Interactive Discussion



## An evaluation of different dry deposition schemes

D. Wen et al.

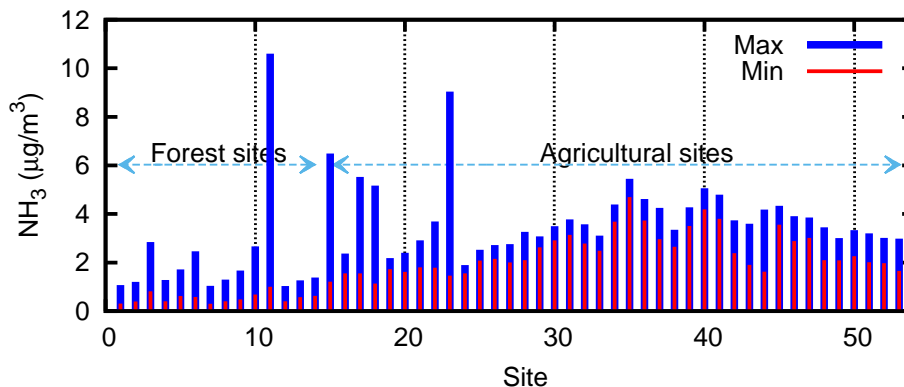


**Fig. 8.** Modeled average  $\text{NH}_3$  concentrations using the set of maximum emission potentials (blue) and using the set of minimum emission potentials (red) for 53 measurement sites. The use of minimum emission potentials is the default.

[Title Page](#)[Abstract](#)[Introduction](#)[Conclusions](#)[References](#)[Tables](#)[Figures](#)[◀](#)[▶](#)[◀](#)[▶](#)[Back](#)[Close](#)[Full Screen / Esc](#)[Printer-friendly Version](#)[Interactive Discussion](#)

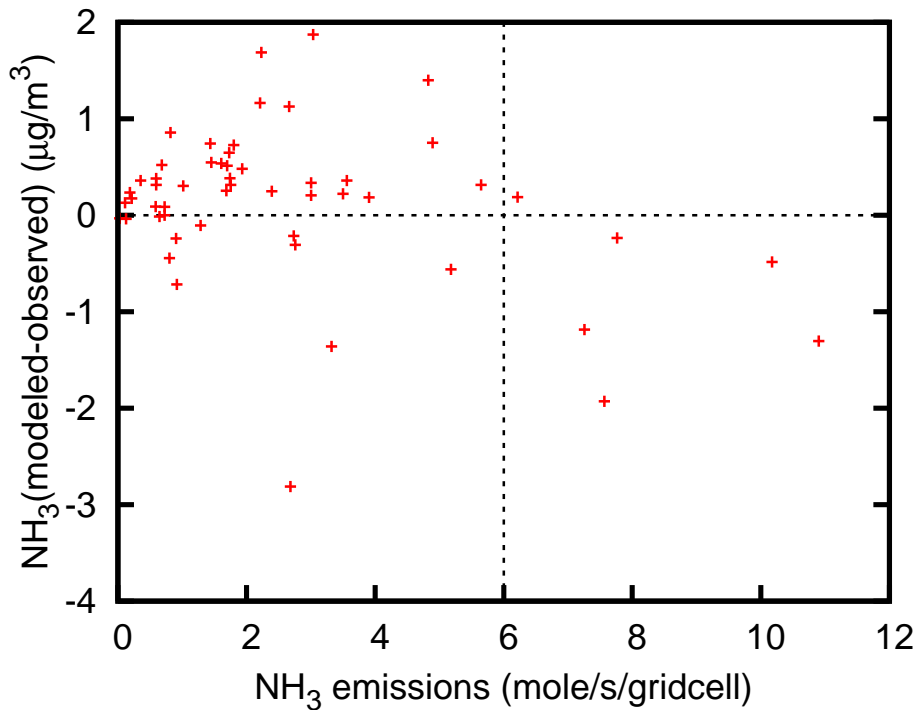


**Fig. 9.** Scatterplot for deviations of modeled NH<sub>3</sub> concentrations from observed values vs. corresponding mean anthropogenic emission strengths for each test sites. All data points are means for the entire simulation period.

**An evaluation of different dry deposition schemes**

D. Wen et al.

Title Page

Abstract

Introduction

Conclusions

References

Tables

Figures

◀

▶

◀

▶

Back

Close

Full Screen / Esc

Printer-friendly Version

Interactive Discussion

